In situ characterization of undulator magnetic fields

Thierry Moreno,* Edwige Otero and Philippe Ohresser

Experience Division, Synchrotron SOLEIL, L'Orme des Merisiers, Saint-Aubin, BP 48, 91192 Gif sur Yvette Cedex, France. E-mail: thierry.moreno@synchrotron-soleil.fr

A new *in situ* method is proposed to characterize the peak magnetic fields of undulator sources. The X-ray beam emitted by the HU52 Apple-2 undulator of the DEIMOS beamline of the SOLEIL synchrotron is analyzed using the Bragg diffraction of a Si(111) crystal. Measurements over the undulator gap range in linear horizontal polarization are compared with simulations in order to rebuild the Halbach function linking the undulator gaps to their peak magnetic fields. The method presented also allows information about the electron beam to be obtained.

Keywords: undulator; crystal Bragg diffraction; Halbach function.

1. Introduction

For undulator beamlines the source is a key element which produces very intense and polarized X-ray radiation owing to its periodic magnetic fields. The undulator is initially assembled and controlled using magnetic measurements (Chubar *et al.*, 2008; Marteau *et al.*, 2009). During this stage the Halbach function (Halbach, 1981) which links the undulator gap to its peak magnetic field is determined for each polarization. Once the undulator is installed in the storage ring, its X-ray emission is characterized through the beamline optical elements. Undulator harmonic calibrations are often performed at constant photon energy by scanning the undulator gap while polarizations are checked at discrete energies using referenced samples. These controls, which can cumulate and combine defects and misalignments of many optical elements, make the proper calibration of the source very complicated.

To bypass this problem, we propose to analyze the undulator emission using a single Si(111) crystal working in Bragg diffraction (Ewald, 2009) and located just after the beamline front-end. The beam diffracted by the crystal is monochromatic and consists of radial concentric harmonics resulting from the interference of the photons emitted by each electron crossing the undulator periods (Kim, 1986; Elleaume, 2003). By comparing the radii of the harmonics measured with the crystal (as a function of the undulator gap) with the ones simulated (as a function of the peak magnetic field), both gap and peak magnetic field can be linked together and the Halbach function determined. Moreover, this method also allows information on the electron beam to be obtained by analyzing the width of the undulator harmonics.

The undulator we have studied is the HU52 Apple-2 undulator (Marteau *et al.*, 2009) of the DEIMOS (Dichroism Experimental Installation for Magneto-Optical Spectroscopy) beamline (Ohresser *et al.*, 2012) of the SOLEIL (Source Optimisée de Lumière à l'Energie Intermédiaire du LURE) synchrotron (Level *et al.*, 2002).

In the first part of this paper we will describe the experimental set-up used to record the undulator harmonic measurements. Then we will show how to relate these measurements to simulations in order to determine the Halbach function and thus characterize the undulator.

2. Experimental set-up

The experimental set-up (Fig. 1) consists of the DEIMOS HU52 undulator under study and the DiagOn (Diagnostic Onduleur) device (Desjardins *et al.*, 2007) that hosts the Si(111) crystal. This device is placed just after the front-end and allows monochromatic images of the undulator radiation to be recorded.

2.1. DEIMOS HU52

The HU52 undulator (Marteau *et al.*, 2009) of the DEIMOS beamline is an Apple-2 undulator (Sasaki *et al.*, 1992; Kobayashi *et al.*, 1996) installed in the I07M medium section of SOLEIL and provides tunable polarization (linear and
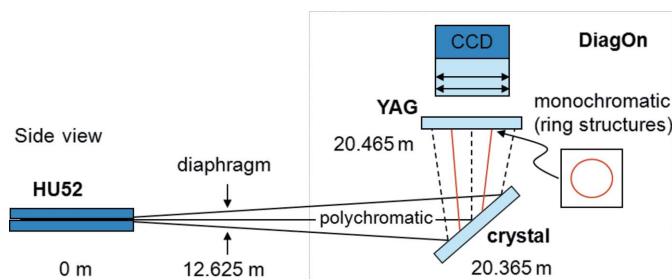
Figure 1
Diagram of the experimental set-up.

research papers

Table 1
HU52 undulator parameters.

Device type	Apple-2
Technology	NdFeB magnets
Field remanence	1.26 T
Period length λ_U	52.4 mm
Number of periods	30 + 2
Minimum gap	15.5 mm
Phase-shift range	−26.2 mm, +26.2 mm

circular) in the spectral range 0.3–3 keV. Table 1 summarizes the main parameters of this undulator. Each magnet block has a size of 28×28 mm transversally and 13 mm lengthways. The gap between consecutive blocks on the same row is 0.1 mm which gives an undulator period of 52.4 mm, whereas transversally the gap between two magnet rows on the same girder is 1 mm.

The Halbach function which links the gap to the peak magnetic field was determined for circular and linear polarizations using magnetic measurements (Marteau, 2008) during the initial assembling and control of the undulator. To adjust these polarizations, the phase shift (Kobayashi et al., 1996) is changed from ±16 mm for circular right and left, 0 mm for linear horizontal (LH) and +26.2 mm for linear vertical (LV).

2.2. DiagOn device

The DiagOn device (Desjardins et al., 2007) was initially developed to align the undulator with the primary diaphragm and is now implemented on all the soft X-ray undulator beamlines at SOLEIL. It consists of a multilayer and a crystal, both reflecting the beam upward in Bragg diffraction on a scintillator screen (YAG:Ce). The images of the beam on the YAG:Ce screen are recorded by a camera. The multilayer and the crystal have been optimized to work for different ranges of gaps according to their diffracted energy, and can be selected using a motorized translation.

In the case of the DEIMOS beamline, the multilayer is made of 100 pairs of Cr(10 Å)/Sc(14 Å) layers and reflects the beam at 367.5 eV according to its Bragg angle of 45°. In LH polarization it targets the first two harmonics of the undulator. The Si(111) crystal reflects the beam at 2796 eV and is used (in LH polarization) to study the undulator harmonics between the third and the 17th. This makes it well adapted for analyzing the undulator properties.

Both optics work in the Brewster condition (grazing angle of 45°), so they polarize linearly the incoming beam. Thus the DiagOn is perfectly adapted to the analysis of the LH undulator polarization (electric field parallel to the synchrotron orbit) but removes almost totally the LV components.

Because the beam diffracted by the optics is monochromatic, the conversion into the scintillator from X-ray to visible light always operates at the same energy, independently of the undulator gap and polarization. The YAG:Ce screen is coated with a 50 nm Cr layer in order to remove the very low energies of the incoming beam reflected by the crystal in specular reflection and produced by the undulator and the bending

magnets located at the two ends of the straight section. According to the DiagOn aperture of 0.3 mrad and its camera magnification of ×0.5, the measurements extend over a detector area of 270×250 pixels (H × V). Before being installed on the beamline, the DiagOn is first calibrated using visible light in order to fix its effective pixel size to a value close to 22 µm. This value can slightly change during the installation owing to mechanical shifts but it is precisely determined through the data analysis process presented in §5.

The multilayer or the crystal absorbs almost all the power transmitted by the working aperture. They are water-cooled on the back and their thermal load must not exceed 250 W (in the present set-up). This limit requires working with gaps above 22.4 m in LH polarization (polarization with the higher power) for apertures of 0.3 mrad.

Future DiagOn improvements are planned, such as using attenuators before the optical system in order to reduce the thermal load and consequently extend the undulator calibration over the full gap ranges, changing the grazing angle of the optics to allow other polarizations than the LH being diffracted and consequently analyzed, and making calibrated marks on the optic in order to directly measure the effective pixel size.

3. Method

The beam emitted by the undulator and diffracted by the Si(111) crystal is monochromatic and consists of radial concentric harmonics (with cone-like shapes), resulting from the interference of the photons emitted by each electron crossing the undulator periods.

The radius θ of the harmonic n is related to the photon energy E and the peak magnetic field B by the following set of equations (Kim, 1986; Elleaume, 2003) (in practical units),

$$K^2 = \frac{1900 \, E_0^2 \, [\text{GeV}] \, n}{\lambda_U \, [\text{cm}] \, E \, [\text{eV}]} - 2\left(1 + \gamma^2 \theta^2\right), \qquad (1)$$

$$K = 0.934 \, \lambda_U \, [\text{cm}] \, B \, [\text{T}], \qquad (2)$$

where E_0 is the energy of the electrons, λ_U is the undulator period and $\gamma = E_0[\text{GeV}]/m_e c^2 = 5831$ at SOLEIL (m_e is the electron mass and c is the velocity of light).

The radii of the harmonics measured (as a function of the undulator gap) are compared with those simulated (as a function of the peak magnetic field). Extending the process over the full gap range allows the Halbach function coefficients, which link the peak magnetic field (B) to the gap (G) of the undulator, to be determined,

$$B = a \exp(bG/\lambda_U), \qquad (3)$$

where a and b are the Halbach coefficients to be set for a fixed undulator polarization.

The harmonic structures of the diffracted beam are strongly dependent on the electron beam properties. Consequently, our simulations, which combine undulator and crystal diffraction calculations, must take into account the emittance and the energy spread of the electron beam.
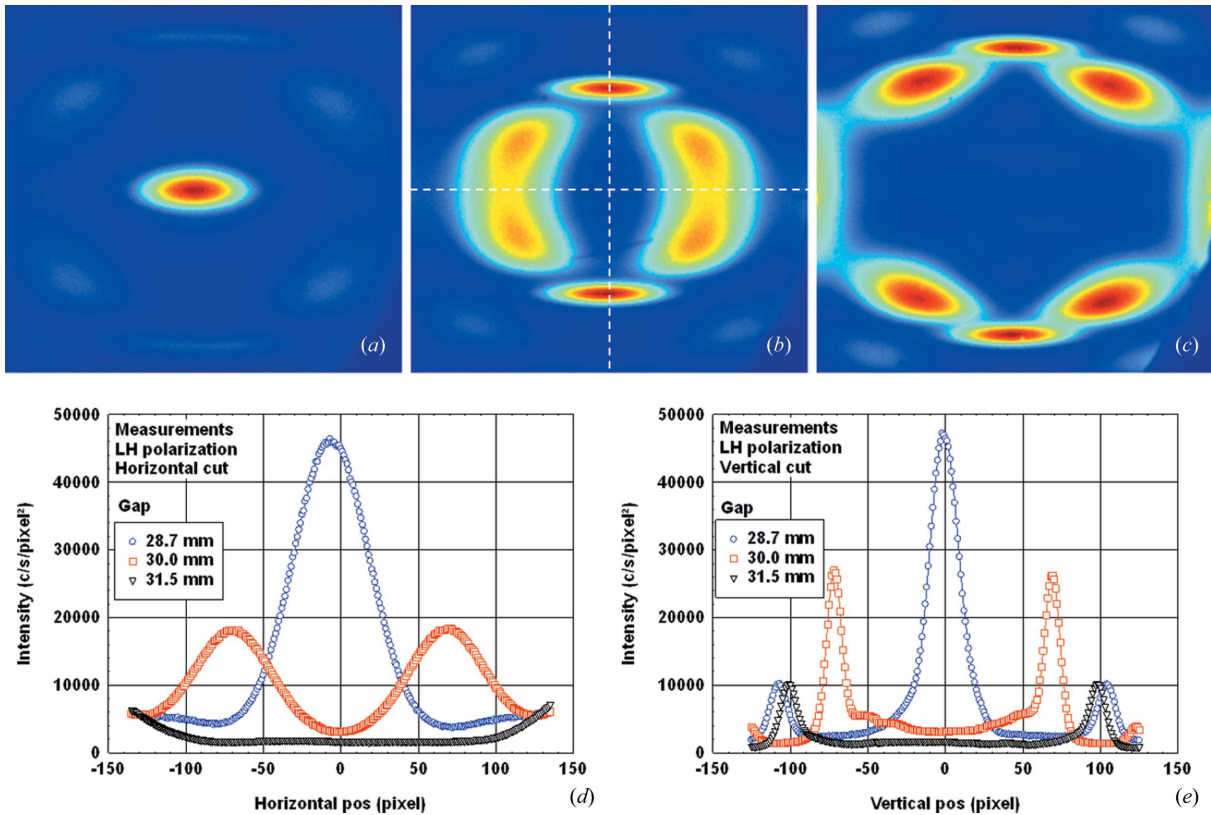
Figure 2
Images and profiles of the beam measured at 2796 eV in LH polarization. Images are recorded for an undulator gap of (*a*) *G* = 28.7 mm, (*b*) *G* = 30 mm and (*c*) *G* = 31.5 mm. In (*d*) and (*e*) the horizontal and vertical, respectively, profiles of the previous images corresponding to the dashed lines in (*b*) are given.

Although the calculations could be achieved through ray tracing (Sanchez de Rio & Dejus, 2004; Schäefers, 2008; Moreno & Idir, 2001) or with a beam propagation code (Chubar & Elleaume, 1998), we chose to develop a dedicated code capable of performing automatically the iterative process of data analysis presented in §5. In this code, undulator radiation properties are evaluated in the far-field case using the Bessel functions expansion (Walker & Diviacco, 1992).

4. Results

Series of measurements using the DiagOn with the Si(111) crystal have been performed with the undulator in LH polarization (phase shift to 0 mm) by varying the undulator gap from 22.4 mm to 50 mm in steps of 0.1 mm.

Fig. 2 shows the images and the profiles of the beam measured at three different gap values along the fifth harmonic of the undulator. The image size is 270 × 250 pixels (H × V). We can see that the radial spots representing the harmonics converge to the center in narrow cones (from right to left on the figure) when decreasing the gap. When the cones are close to the edge or to the center of the detector area, the harmonic structures are poorly defined and lead to errors in the measurements.

The angular radius and width of the harmonics were determined using Gaussian fits for all the measurements in both the horizontal and the vertical direction according to the dashed lines in Fig. 2(*b*). Fig. 3 shows the result of these fits for the LH polarization covering the third to the eighth harmonic.
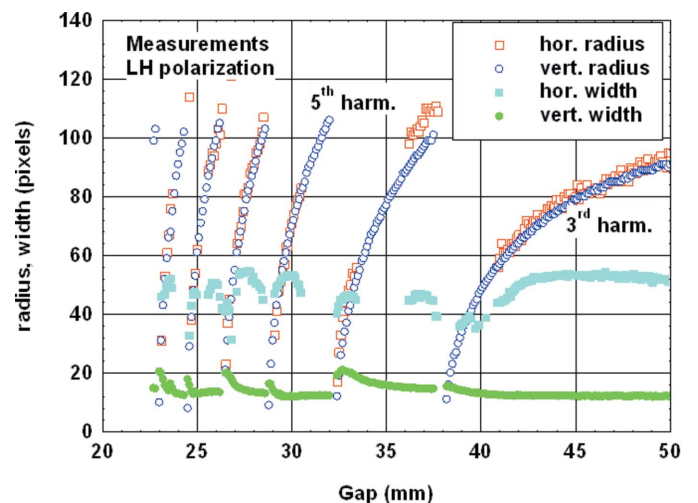
Figure 3
Measurements of the horizontal and vertical radius and width (in pixels) of the third to the eighth harmonic *versus* the gap in LH polarization.
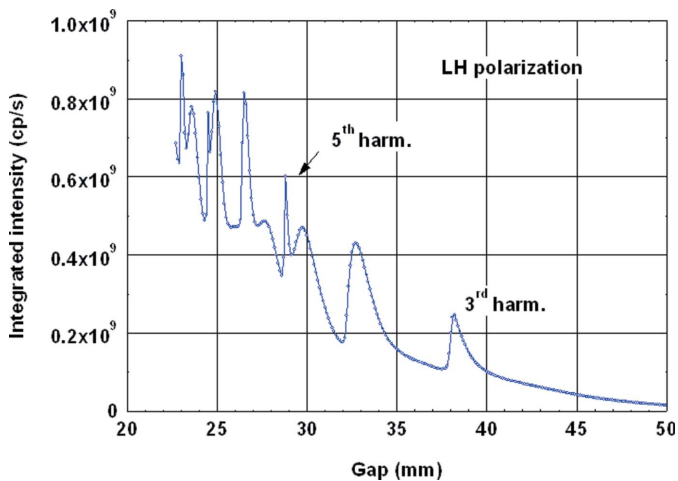
Figure 4
Gap scan measured at 2796 eV in LH polarization *versus* the integrated intensity.

The radius of each harmonic converges to the axis of the undulator when the gap is closing. Because of their narrow sizes, the vertical structures are well defined almost over the full detector area while horizontally this area does not exceed 90 pixels (as we can see in the angular radius discrepancies on the top of the fourth harmonic).

The vertical width of each harmonic is almost constant with the gap except when the harmonic reaches the center of the image and its shape changes from radial to Gaussian [see Figs. 2(a) and 2(b)]. Because it is far bigger than the vertical, only the horizontal width is well defined and almost constant in very small areas depending on the harmonic structure modulations. In well defined areas, as in the case of a 43 mm gap, the vertical and horizontal widths are 12.1 and 53.0 pixels FWHM, respectively.

The integration time was adapted during the gap scan to avoid saturated images and to benefit from the full sensitivity of the camera over the gap range. Fig. 4 shows the resulting gap scan at 2796 eV obtained by integrating all the measured images.

In order to compare the previous experimental measurements with the theory, we have calculated the harmonic structures of the beam as a function of the peak magnetic field in LH polarization. Fig. 5 shows the variations of the calculated radius and width (vertical and horizontal profiles) as a function of the peak magnetic field for the third to the eighth harmonic.

In the simulations we take into account the emittance and energy spread of the electron beam and the Bragg diffraction of the Si(111) crystal. As the conversion from X-rays to visible in the YAG:Ce screen operates mainly at fixed energy (2796 eV), the YAG fluorescence is considered in the simulations as a constant parameter. Similarly to the experimental measurements (Fig. 3), discrepancies appear between the horizontal and the vertical radius of the harmonics owing to both the electron beam convolution and the edge image effects. For each harmonic, simulated widths are essentially constant in the image area where the structures are well
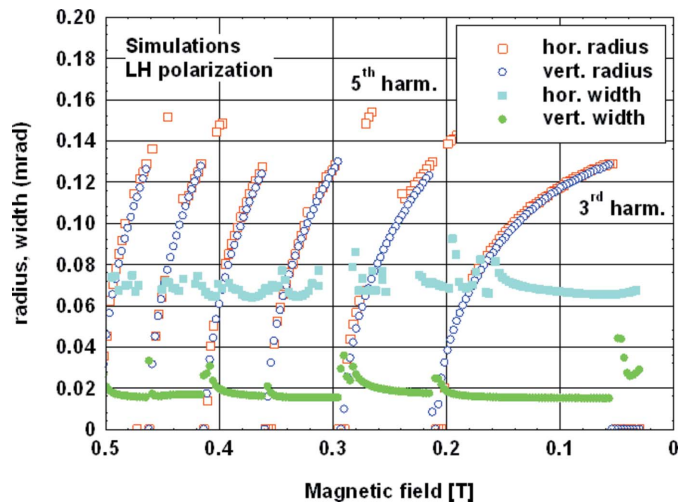
Figure 5
Simulations of the horizontal and vertical radius and width (in mrad) of the third to the eighth harmonic *versus* the peak magnetic field in LH polarization. Even if the even harmonics vanish when reaching the undulator axis, they still are well defined with radii below 0.01 mrad in LH polarization in spite of their very small intensity.

defined, *i.e.* outside the center and edges of the detector plane.

5. Characterization of the Halbach function in LH polarization

The idea is to link for each harmonic the angular radii measured as a function of the gap (Fig. 3) to those calculated as a function of the peak magnetic field (Fig. 5) in order to obtain the Halbach function. The connection between both the measured and the calculated curves is made for each harmonic using the effective pixel size, which is a geometrical factor converting angular distributions in mrad (from simulations) into spatial distribution in pixels (on the detector plane).

This geometrical factor depends mainly on the magnification of the DiagOn imaging system and its distance from the undulator center. Nevertheless, discrepancies between the measured and the simulation conditions, such as different polarization ratio or undulator manufacturing defects (not taken into account in the simulations), can also modify this factor. Because they are better defined over a larger area, we use the vertical radii (of Figs. 3 and 5) instead of the horizontal to determine the Halbach functions associated with each harmonic.

The best effective pixel size is obtained when the Halbach functions associated with each harmonic are aligned together. Fig. 6 shows, in the gap range 22.4–46 mm, the resulting curves for both the best effective pixel size of 24.65 μm and, for comparison purpose, an effective pixel size of 22 μm which produces a discontinuous set of harmonic functions.

In practice, the dispersion of these functions is minimized through the exponential fit of the peak magnetic field. This dispersion results mainly from the errors in the measure of the vertical radius of the harmonics (Fig. 3) which is 0.34 pixel
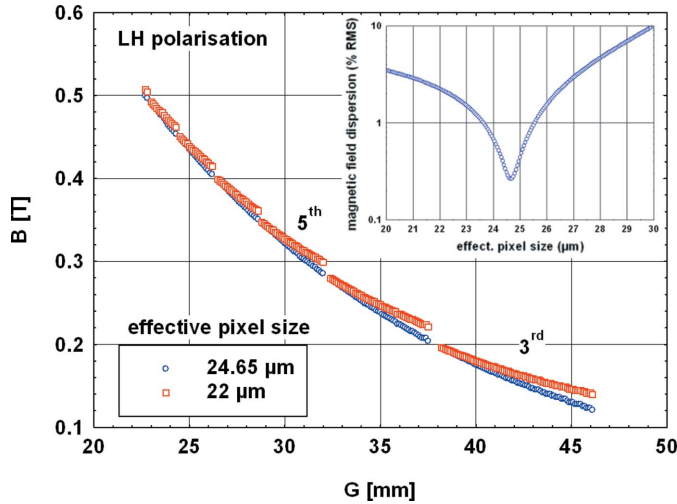
Figure 6
Resulting Halbach functions for two effective pixel values. The minimum gap for each function corresponds to the on-axis harmonic configuration. The inset curve shows, as a function of the effective pixel, the magnetic field dispersion (% RMS) of these functions in LH polarization.

RMS (0.47% RMS) and the error in the value of the energy of diffraction which is 3.1 eV RMS (0.11% RMS) resulting from the accuracy of the crystal angle ($\pm 0.1°$). Other geometrical parameters such as the position and the magnification of the DiagOn are comprised in the effective pixel size evaluation and do not take part in the magnetic field dispersion.

In the best-fit configuration (24.65 μm pixel^{-1}) the error of the magnetic field is 5.5×10^{-4} T RMS (0.30% RMS). The resulting Halbach coefficients are $a = 1.976$ T (with an RMS error of 4.5×10^{-3} T = 0.23%) and $b = -3.1702$ (with an RMS error of 5.5×10^{-3} mm^{-1} = 0.17%). These coefficients are similar within the error bars to those obtained from the magnetic measures (Marteau, 2008), $a = 1.974$ T and $b = -3.1754$ (obtained for measured magnetic fields with RMS errors below 0.3%), which show that our method can converge to the real Halbach coefficients.

This effective pixel size also sets the size of the detector area to 6.64×6.15 mm (H $\times$ V) which allows a direct comparison between measures and simulations for individual gaps and consequently the evaluation of the effect of the electron beam emittance on the harmonic structures.

It is assumed that the electron beam size and divergence have a Gaussian distribution, thus the resulting harmonic widths σ_H on the detector plane can be defined by

$$\sigma_H^2 = \sigma^2 + L^2(\sigma'^2 + \sigma_\theta^2), \qquad (4)$$

where σ and σ' are the electron beam size and divergence, respectively, L is the distance between the center of the undulator and the detector plane, and σ_θ is the photon divergence.

Using the relation (4) with the machine electron beam parameters for DEIMOS (Table 2), a detector plane distance of $L = 20.465$ m and a photon divergence $\sigma_\theta = 1.2$ μrad RMS (which is typical for such detector aperture), we expect hori-

Table 2
Electron beam parameters (medium section).

Horizontal size σ_x	182 μm RMS
Vertical size σ_z	8.1 μm RMS
Horizontal divergence σ'_x	30.5 μrad RMS
Vertical divergence σ'_z	4.6 μrad RMS

zontal and vertical harmonic widths of 1529.0 μm FWHM and 229.4 μm FWHM, respectively.

On the other hand, by applying the effective pixel size of 24.65 μm to the LH measurements displayed in Fig. 3, the horizontal and the vertical harmonic widths are 1303.8 μm FWHM and 297.7 μm FWHM, respectively, which means a difference of -15% horizontally and of $+30\%$ vertically with respect to the widths obtained using the machine electron beam parameters (Table 2).

Relation (4) does not allow the electron beam size and divergence to be separated. Because of the small vertical source size and the large distance between the source and the detector plane, the vertical harmonic width [relation (4)] mainly depends on the electron beam divergence while horizontally both the electron beam size and divergence strongly participate in the harmonic spread. Assuming the machine electron beam size of Table 2, the measured divergence becomes 25.5×6.0 μrad RMS (H $\times$ V) (instead of 30.5×4.6 μrad RMS as defined by the machine). Using these electron beam parameters, Fig. 7 shows the simulated beam profiles related to the measures displayed in Fig. 2, corresponding to the fifth harmonic in LH polarization.

These simulated images compare very well with the measured images presented in Fig. 2, in spite of the presence of a background appearing on the measurements. This background varies with the undulator gap and comes essentially from the intensity emitted incoherently by the undulator owing to its phase errors and the two entry/exit half magnetic fields of the undulator (not taken into account in the simulations). The ratio between the intensities measured [Figs. 2(d) and 2(e)] and simulated [Figs. 7(d) and Fig. 7(e)] is 4.6×10^4, and it results from the fluorescence process efficiency in the YAG:Ce screen, the aperture stop of the camera and the CCD sensitivity.

6. Conclusion

In this paper we have presented a new method of determining *in situ* the magnetic properties of an undulator. We use Bragg diffraction with a crystal to obtain monochromatic structures of the undulator X-ray emission. These structures are compared with simulations in order to retrieve the Halbach function, relating the peak magnetic field to the undulator gap. The Halbach coefficients deduced from our method are identical within the error bars to the values obtained from the *ex situ* magnetic measurements. This result confirms that our method is indeed able to characterize *in situ* an undulator. This will give the opportunity for beamlines to have a facility for surveying their source.
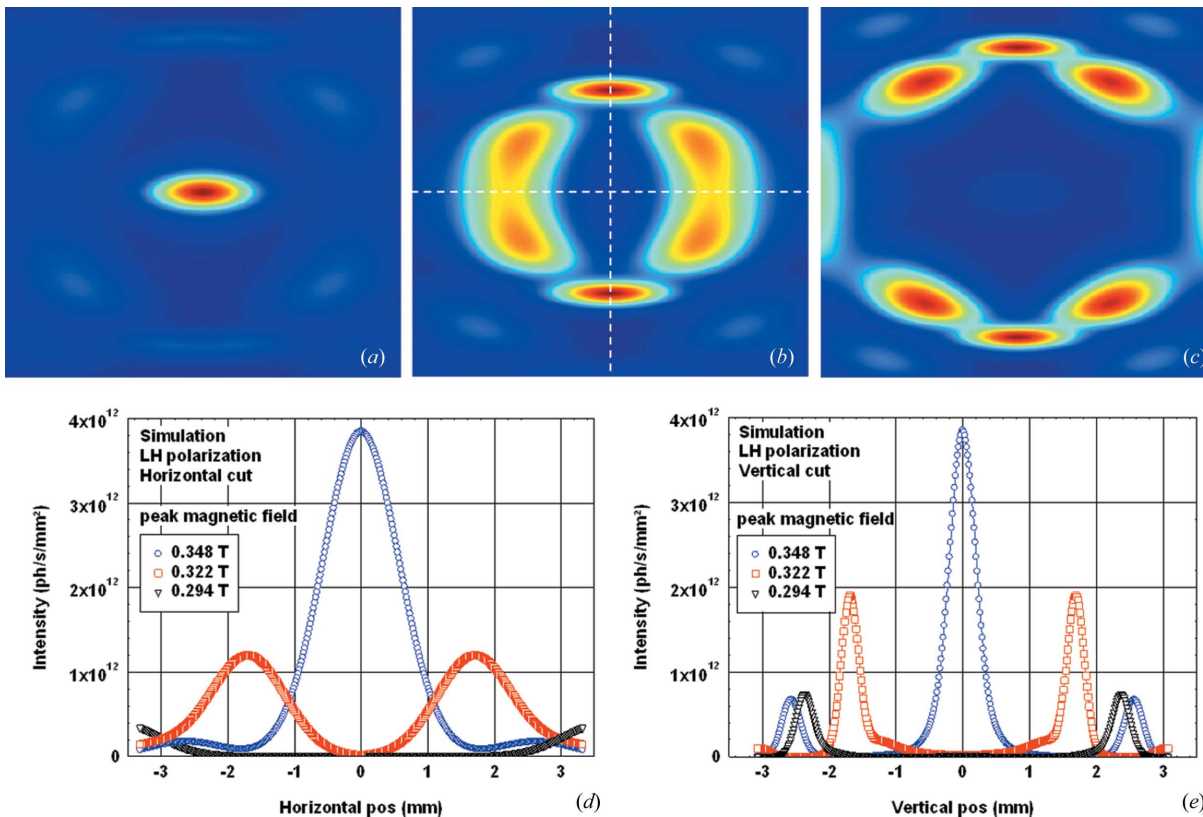
Figure 7
Simulation of the measured structures displayed in Fig. 2 using an electron beam size of 188 × 8.2 μm RMS (H × V) and divergence of 25.5 × 6.0 μrad RMS (H × V). The image area is 6.64 × 6.15 mm (H × V). Images are calculated for a peak magnetic field of (a) $B = 0.348$ T corresponding to a gap of $G = 28.7$ mm, (b) $B = 0.322$ T corresponding to $G = 30$ mm and (c) $B = 0.294$ T corresponding to $G = 31.5$ mm. In (d) and (e) the horizontal and vertical, respectively, profiles of the previous images corresponding to the dashed lines in (b) are given.

References

Chubar, O., Briquez, B., Couprie, M.-E., Filhol, J.-M., Leroy, E., Marteau, F., Paulin, F. & Rudenko, O. (2008). *Proceedings of the 11th European Particle Accelerator Conference (EPAC'08)*, pp. 2246–2248.

Chubar, O. & Elleaume, P. (1998). *Proceedings of the Sixth European Particle Accelerator Conference (EPAC'98)*, pp. 1177–1179.

Desjardins, K., Hustache, S., Polack, F., Moreno, T., Idir, M., Dubuisson, J.-M., Daguerre, J.-P., Giorgetta, J.-L., Thoraud, S., Delmotte, F. & Ravet-Krill, M.-F. (2007). *AIP Conf. Proc.* **879**, 1101–1104.

Elleaume, P. (2003). *Brunnen 2003, Synchrotron Radiation and Free-Electron Lasers*, edited by D. Brandt, pp. 83–119. Geneva: CERN.

Ewald, F. (2009). *Proceedings of the 9th European Workshop on Beam Diagnostics and Instrumentation for Particle Accelerators (DIPAC09)*, pp. 182–184.

Halbach, K. (1981). *Nucl. Instrum. Methods Phys. Res. A*, **187**, 109–117.

Kim, K. J. (1986). *Nucl. Instrum. Methods Phys. Res. A*, **246**, 67–70.

Kobayashi, H., Miyahara, Y., Sasaki, S., Shimada, T., Takao, M. & Yokoya, A. (1996). *Proceedings of the 1996 European Particle Accelerator Conference (EPAC96)*, pp. 2579–2581.

Level, M.-P., Brunelle, P., Chaput, R., Filhol, J.-M., Herbeaux, C., Loulergue, A., Marcouille, O., Marlats, J.-L., Nadji, A. & Tordeux, M.-A. (2002). *Proceedings of the Eighth European Particle Accelerator Conference (EPAC'02)*, pp. 212–214.

Marteau, F. (2008). Personal communication.

Marteau, F., Benabderrahmane, C., Berteaud, P., Briquez, F., Brunelle, P., Chapuis, L., Couprie, M.-E., ElAjjouri, T., Filhol, J.-M., Kitegi, C., Marcouille, O., Massal, M., Nadji, A., Nadolski, L. S., Nagaoka, R., Tavakoli, K., Valleau, M., Veteran, J. & Chubar, O. (2009). *Proceedings of the 23rd Particle Accelerator Conference (PAC09)*, pp. 2453–2455.

Moreno, T. & Idir, M. (2001). *J. Phys. IV Fr.* **11**, 527–531.

Ohresser, P., Otero, E. & Choueikani, F. (2012). In preparation.

Sanchez del Rio, M. & Dejus, R. J. (2004). *AIP Conf. Proc.* **705**, 784–787.

Sasaki, S., Miyata, K. & Takada, T. (1992). *Jpn. J. Appl. Phys.* **31**, 1794–1796.

Schäefers, F. (2008). *RAY – The BESSY Ray-Trace Program*, Version 24.5.2008. BESSY, Berlin, Germany.

Walker, R. P. & Diviacco, B. (1992). *Rev. Sci. Instrum.* **63**, 392–395.